Physical Archaeology

The energy from an LENR event is sufficient to melt a 100 nm bubble of PdD or vaporize a 50 nm one. Damage on these size scales should be detectable, especially if it occurs near the surface of the material, where it can be imaged. Physical archaeology refers to looking for these physical scars, which energy from an LENR event will leave behind in the material.

We have gone through three evolutions in learning how to look for LENR using this approach; all based upon SEM imaging in order to provide high resolution imagery over relatively large areas. Here we compare SEM images of the sample before and after the experiment, looking for damage caused by the experiment.

Initial Approach

In our initial approach, we focused on free standing, bulk sample geometries (e.g., Pd foils and slugs). Native Pd sample surfaces (i.e., as received) are too noisy to make useful interpretations. So, we developed mechanical polishing and chemical cleaning techniques to prepare pristine Pd surfaces prior to AHE experiments (**Fig 1**). However, loading significantly distorts the sample surface, convoluting SEM image data. We developed the elastic loading technique to uniformly load, but the presence of grain boundaries in polycrystalline Pd still led to distortions such as intergranular voids and cracks, grain growth and terracing. So, we switched to single crystal Pd samples, which successfully mitigated the distortions driven by grain boundaries and preserved the pristine surface after elastic loading and deloading (**Fig. 2**).

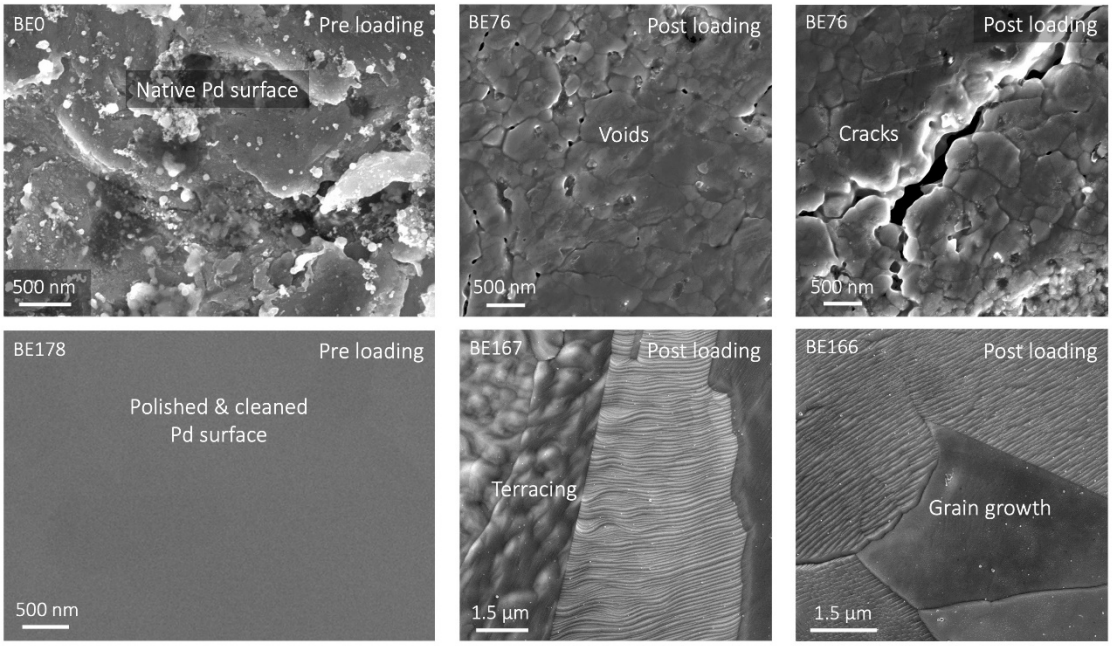

Fig. 1: (Top left) Native polycrystalline Pd surfaces are rough and full of debris / contamination. (Top center and right) Even polished samples become distorted by loading/deloading. (Bottom left) After mechanically polishing and chemically cleaning, the Pd surfaces are pristine. (Bottom center and right) However, post elastic loading, polycrystalline surfaces are distorted (e.g., intergranular voids and cracks, grain growth, and terracing), primarily due to the presence of grain boundaries.

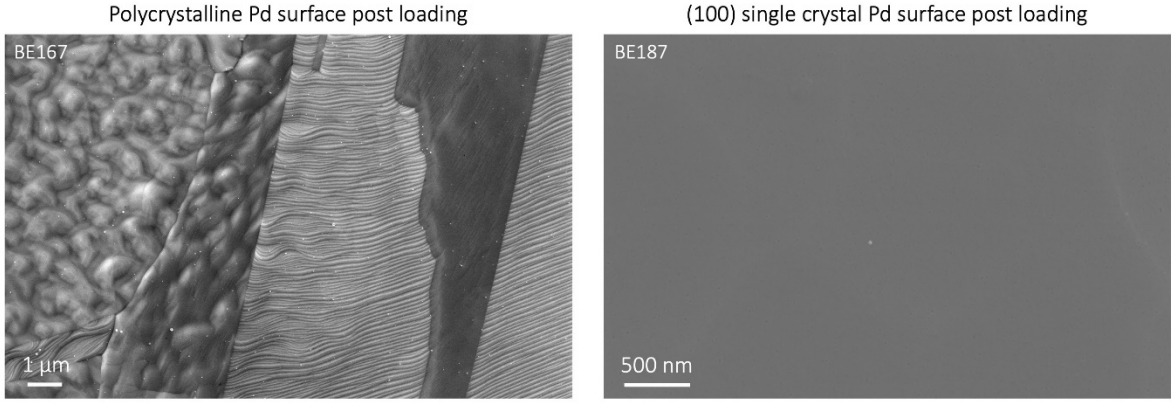

Fig. 2: Single crystal Pd surfaces remain pristine after elastic loading and deloading, successfully mitigating the distortions driven by grain boundaries in polycrystalline Pd.

Beyond developing sample preparation and loading techniques to preserve the sample surface, cleanliness is essential for valid archaeology data i.e., debris / contamination can obscure SEM images. As an example, we observed “linear features” (LFs) in early experiments. The LFs were

observed in both protium and deuterium with varying dimensions and concentrations (**Fig. 3**). LFs tended to appear in areas with nanoparticle contamination (aluminum oxide, Al_2O_3, nanoparticles were used to mechanically polish the samples prior to the experiments and were not entirely removed). Initial EDS (energy dispersive x-ray spectroscopy) analysis was unable to identify the chemical composition of the LFs due to the strong background signal of the Pd sample (i.e., when the LFs were on the Pd surface, the EDS only identified Pd). So, we used an in-situ manipulator to pick a LF off the Pd surface and perform EDS in isolation. This clearly showed the LFs were AlF_3 and most likely generated from a reaction of the Al_2O_3 nanoparticles and F from the lubricants in the pressure source (**Fig. 4**). Thus, archaeology relies on clean, contaminate-free surfaces to yield useful insights and avoid needless rabbit holes.

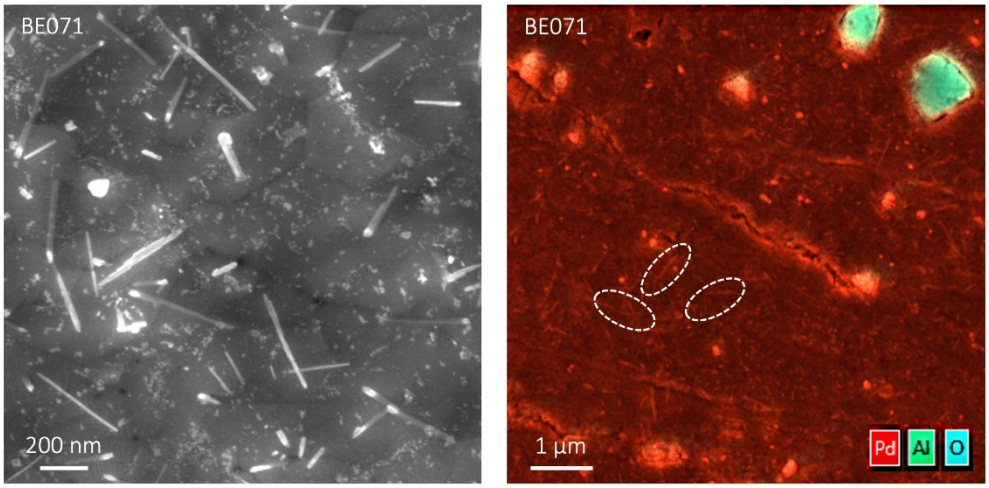

Fig. 3: Linear features (LFs) were identified on both protium and deuterium loaded Pd surfaces. EDS was unable to chemically distinguish LFs from the background Pd signal.

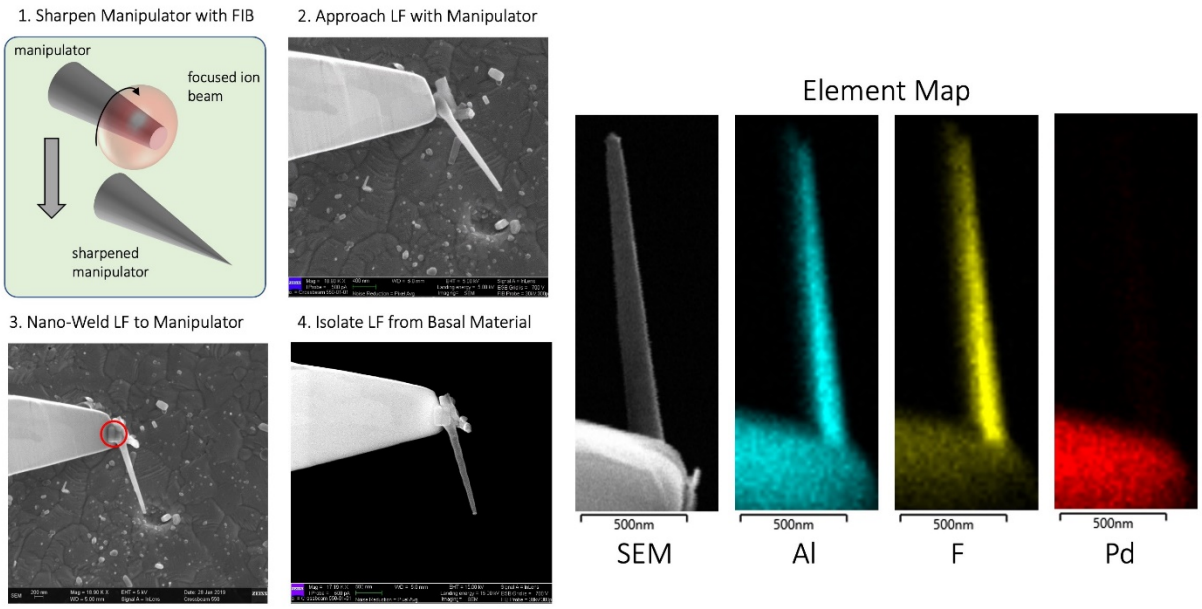

Fig. 4: Using a micromanipulator, a LF was picked off the Pd surface and EDS imaged in isolation, clearly revealing the LFs composition: AlF_3.

A final learning from the initial physical archaeology campaign was the importance of avoiding supercontinuum generation in our short-pulsed laser stimulation experiments. Using a Coherent Astrella short-pulsed laser with < 50 fs pulse durations at wavelengths of 400nm and 800nm, we performed stimulated AHE experiments at loadings >0.9 in Pd/D(H) and used pre/post SEM imaging as our AHE diagnostic. Valid stimulation experiments require fluences below the Pd/D(H) damage threshold, so as not to convolute laser damage with AHE damage sites (we expected 24 MeV AHE events to leave ~100nm voids/melt-spots in the Pd surface). We did observe ~100nm melt spots on some PdD_x samples (**Fig. 5**), but it was inconsistent (i.e., using identical loading and pulse conditions, we did not always observe the melt spots). We confirmed with cross sections that the melt spots were accompanied with sub-surface < 100nm voids (**Fig. 6**). We found that our samples were too close to our pressure windows and our focused, short-pulse beam was undergoing a non-linear optical effect that non-uniformly broadened the spectrum of incident light called supercontinuum generation (**Fig. 7**). This created illumination conditions that inconsistently damaged our samples. By increasing the sample-to-window distance, we avoided supercontinuum generation and confirmed that the melt-spots were in-fact laser damage (**Fig. 8**). So, clean archaeology experiments with short-pulse laser stimulation must avoid supercontinuum generation and stimulate below damage threshold.

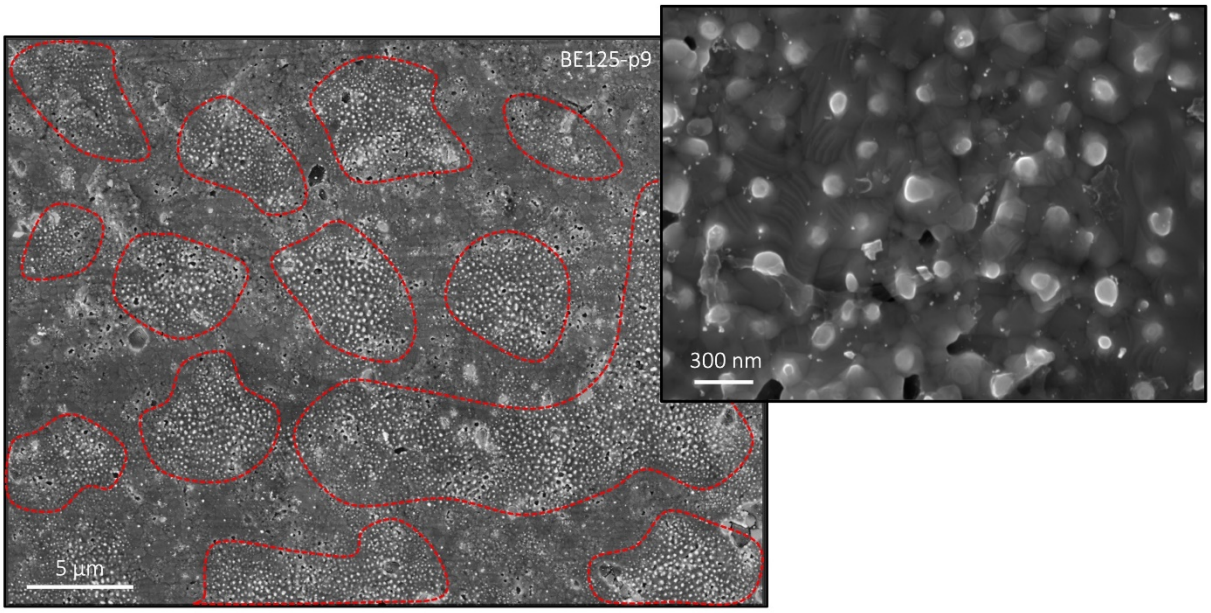

Fig. 5: Some PdD_x samples displayed patches of ~100nm melt spots after stimulation, but it was inconsistent.

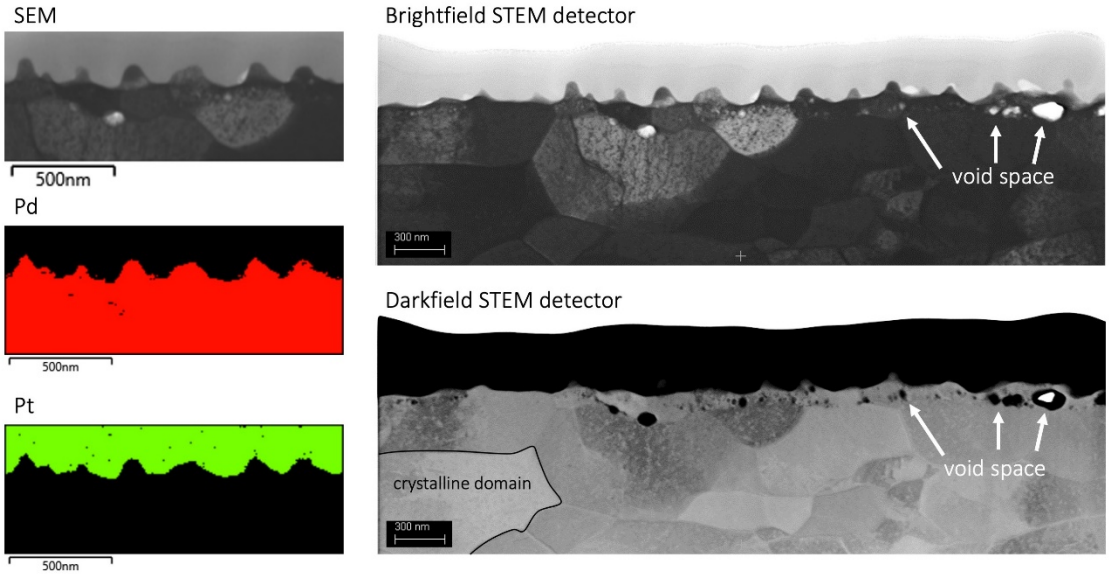

Fig. 6: The melt spots in PdD_x samples were accompanied by sub-surface <100nm voids.

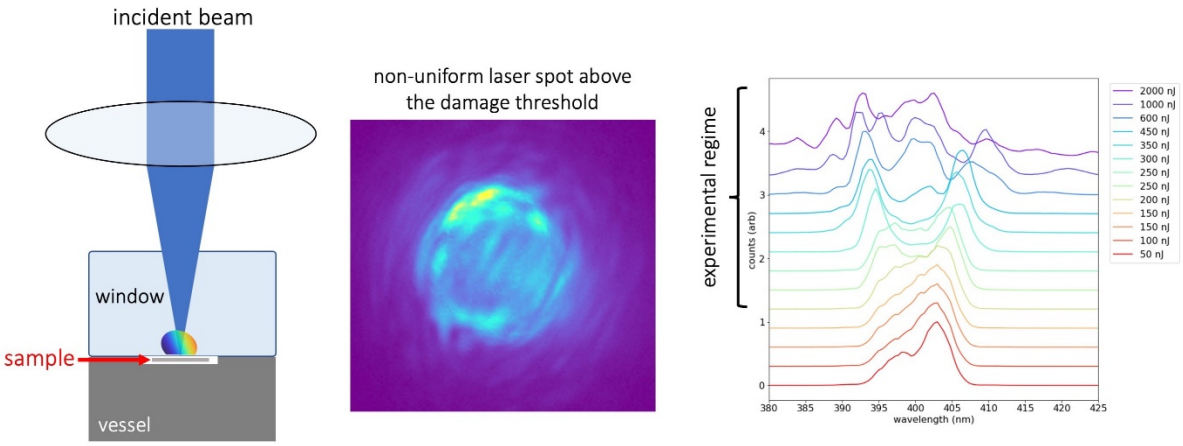

Fig. 7: With samples in close proximity to thick pressure windows, a focused, short-pulse beam can undergo supercontinuum generation and create inconsistent illumination conditions.

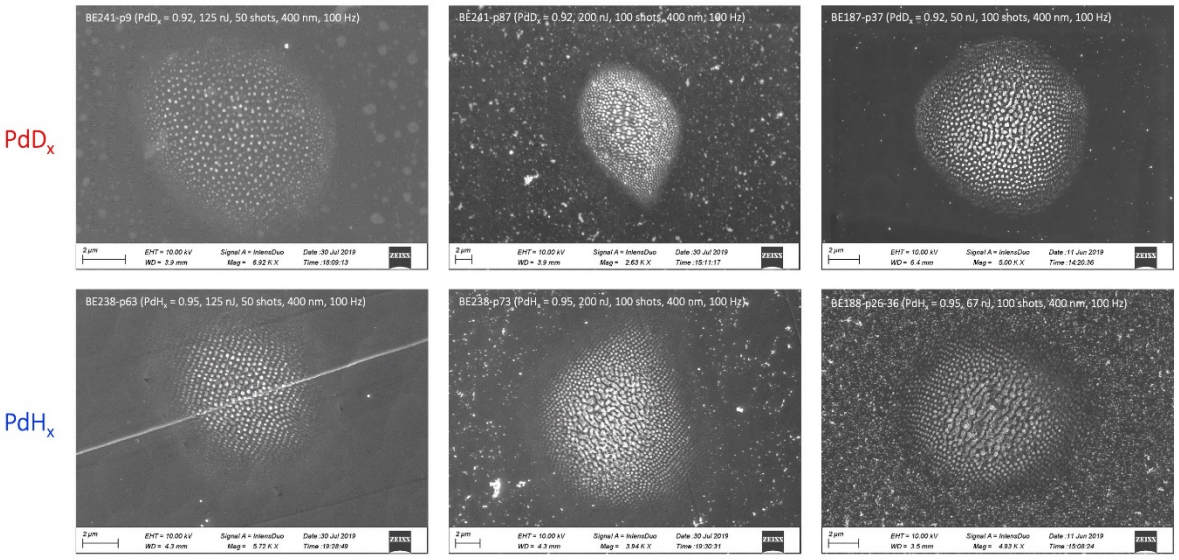

Fig. 8: Increasing the sample-to-window distance avoids supercontinuum generation and yields reproducible damage spots across PdD_x and PdH_x.

Nanostructure Archaeology

Following our initial archaeological approach, we switched our efforts to nanostructured targets, where damage would be more apparent. One key advantage is achieved by fielding nanostructures small enough so that the heat from an AHE event will damage or destroy them. This is done by

keeping their size (in at least one direction) well below 100 nm. A second way to make damage more visible, was to use arrays of discrete nanostructures. Not only is damage often more apparent in a small nanostructure, but they provide the damage sites with clearcut addresses; researchers can agree on locations for additional commentary or inspection.

Nanostructure Archaeology : Nanopillar Arrays

Our first, and most technologically most sophisticated, type of nanostructures developed for archaeology were Pd nanopillars. Each of these was a small cylindrical pillar, typically 60 - 100 nm wide and about 200 nm tall. The concept behind them is shown below; energy from a single 24 MeV AHE event will be spatially confined by their small diameter, and severely damage, if not destroy, the pillar.

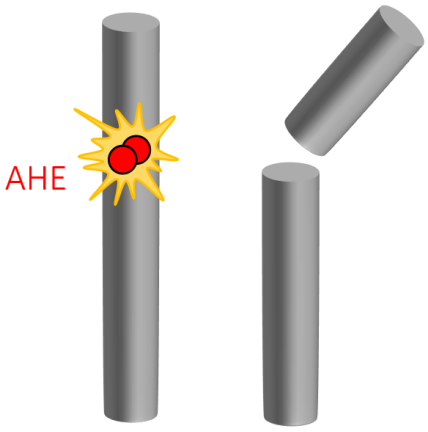

Two other characteristics of Pd nanopillars are worth noting. Because of their small dimensions, they load (and deload) with deuterium very quickly. And, since they are only anchored at their base, most of the swelling caused by deuterium loading is unrestrained, so does not cause internal stresses or disruptions to the Pd lattice.

Obviously, a problem with nanopillars is that they are small. So, in order to test a significant amount of PdD material, we need to field a very large number of nanopillars. We did so by creating large 2D arrays of nanopillars on a substrate, typically containing millions of individual pillars.

Nanopillar arrays were first formed by sculpture, carving them out of bulk Pd samples by using focused ion beam (FIB) milling (**Fig. 9, Fig. 10**). First, 0.5mm thick, 5.5mm diameter 'slugs' were fabricated from mono-crystalline rods of palladium and their surface was polished to nanometer or sub-nanometer scale surface roughness via chemical mechanical polishing and grazing incident Ar^{+} ion milling. The pristine surfaces were laser marked with fiducials to measure sample strain during loading and target boxes which could be targeted by stimulation lasers in experiments.

Finally, a gallium FIB column in an SEM was programed to mill recessed arrays of nano pillars into the sample surface within the target boxes.

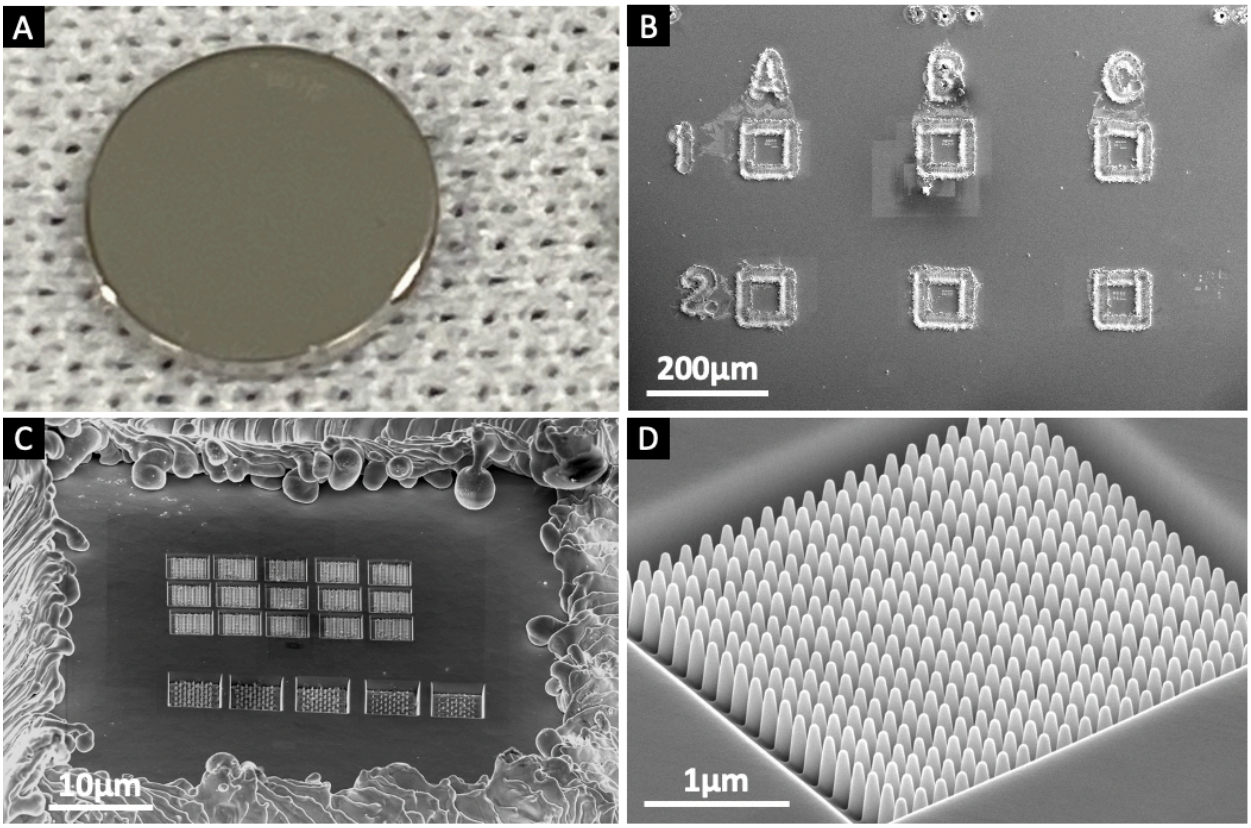

Figure 9. A) A single crystal palladium slug polished to sub-nanometer RA surface roughness. B) Laser marked target pads shown on the surface of the palladium slug. C) A target pad containing 20 FIB pillar arrays. Each array utilized slightly different milling conditions or programmed milling pattern to generate an assortment of pillar geometries and array layouts on each pad. D) A FIB pillar array containing 400 individual palladium nano pillars.

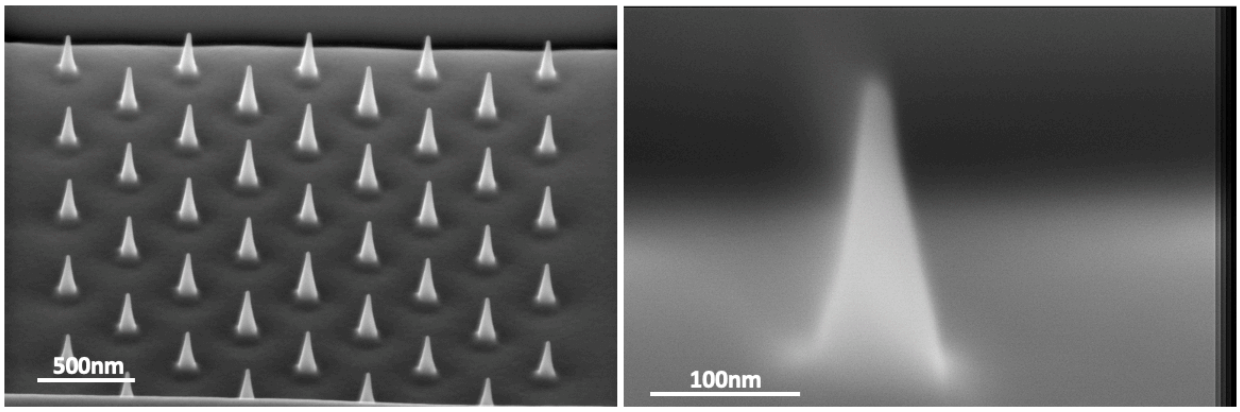

Figure 10. The size of FIB pillars could be decreased by further exposure to the ion beam.

During short pulse stimulation of deuterium loaded targets containing FIB pillars, archaeology found evidence of altered pillars (**Fig. 11**). However, this result was eventually replicated in protium and was therefore determined to be an effect of classical origin, not a result of LENRs.

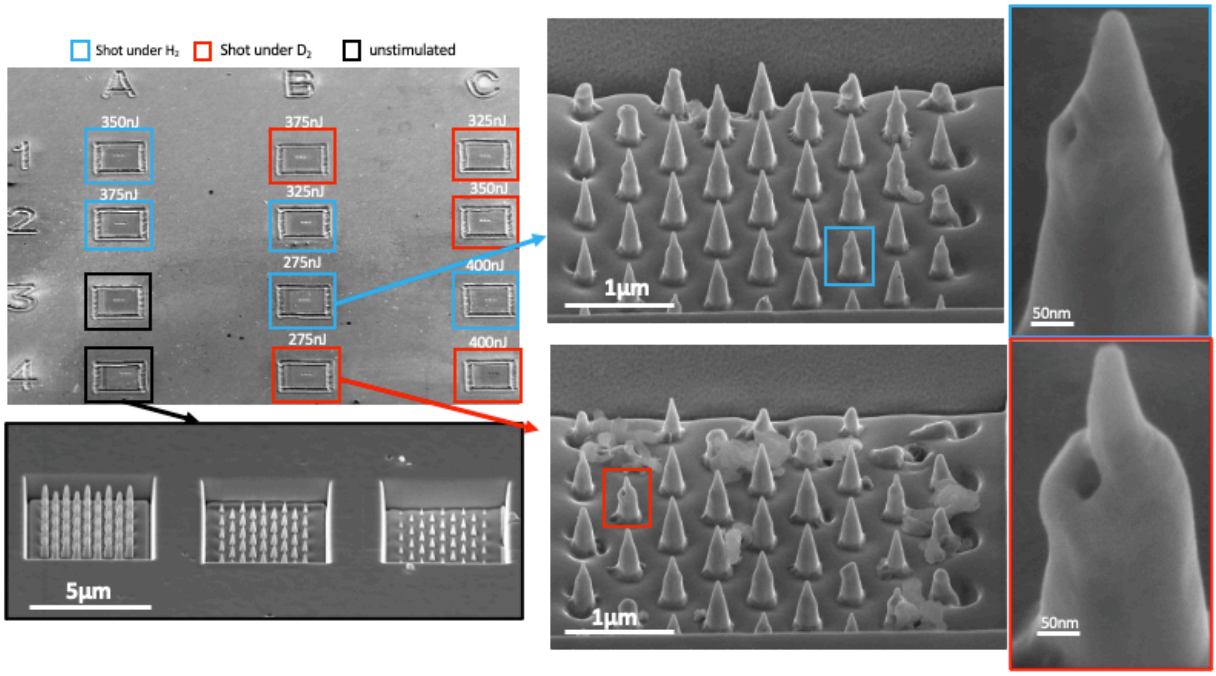

Figure 11. Callisto experiment BE827. FIB nanopillars on single crystal Pd are loaded at ultrapressure (H_2/D_2) and stimulated using a high fluence, ultra-short pulse laser. Pillars illuminated by 275nJ pulse energy exhibited cavities and other structural changes in the archaeology analysis. The effect was produced under both hydrogen and deuterium and was found to be not isotopically dependent.

Milling pillars using FIB is a time intensive process which limits the number of pillars on each sample. A more scalable approach was developed using electron beam lithography to pattern arrays of holes in a resist layer on gold coated silicon wafers (**Fig. 12**). Palladium was then electroplated onto the wafer to form palladium nanopillars in the holes. Extensive effort was required to optimize the lithography process for hole diameter and uniformity of the resulting arrays. Lower e-beam doses and development time lead to smaller diameter holes/pillars but risk residual resist at the base of the hole preventing wetting during electroplating, leading to missing pillars within the array. Through extensive testing, a process for wetting and plating the proper palladium thickness was achieved.

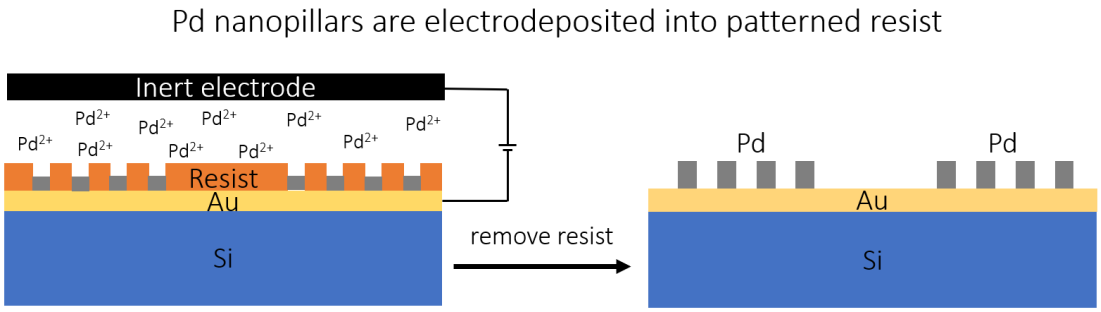

- Electrodeposition is commonly used to fill vias in the semiconductor industry; Plating vias on the nanoscale is more challenging due to the need for e-beam lithography
- We developed a method to plate nanoscale vias with near-perfect uniformity and reproducibility down to 60nm

Figure 12. Pd nanopillar fabrication procedure.

The nanopillars arrays (**Fig. 13**) formed hexagonal patterns, with 400 nm spacing between nanopillars. Most of these arrays were intended for use with laser stimulation, so were patterned into a 3x3 array of separate nanopillar-filled pads, spaced apart so that each pad could be irradiated with different stimulation conditions. Each pad was 250 microns on a side, and contained 450,000 nanopillars; so there were over 4,000,000 pillars in a typical experiment. Substrates were prepared by evaporating 10nm titanium followed by 150nm gold onto Si wafers. The wafers were then coated in 300nm thick PMMA 950k and large cross marks near the corner of the wafer were exposed using DUV and a physical mask. The large cross marks had a combined area of 1cm^2 and accounted for the overwhelming majority of the exposed gold, making the current density in the holes much more stable and controllable during electroplating. The virtual mask for e-beam lithography contained 30nm wide hexagons to define each pillar and was exposed onto the PMMA resist with a dose typically between 3,000 and 5,000$\mu C/cm^2$. The pattern was then developed and descummed using 15s O_2 plasma following development, and again before electroplating. Wafers were pre-wet by submerging in $PdCl_2$ based electroplating solution in a vacuum chamber for 5 minutes. Electroplating was typically done using constant current at 10mA with plating times ranging from 30 seconds to 2 minutes. After electroplating, wafers were diced using a micromachining laser and cleaned with a series of solvents including acetone to remove the PMMA resist.

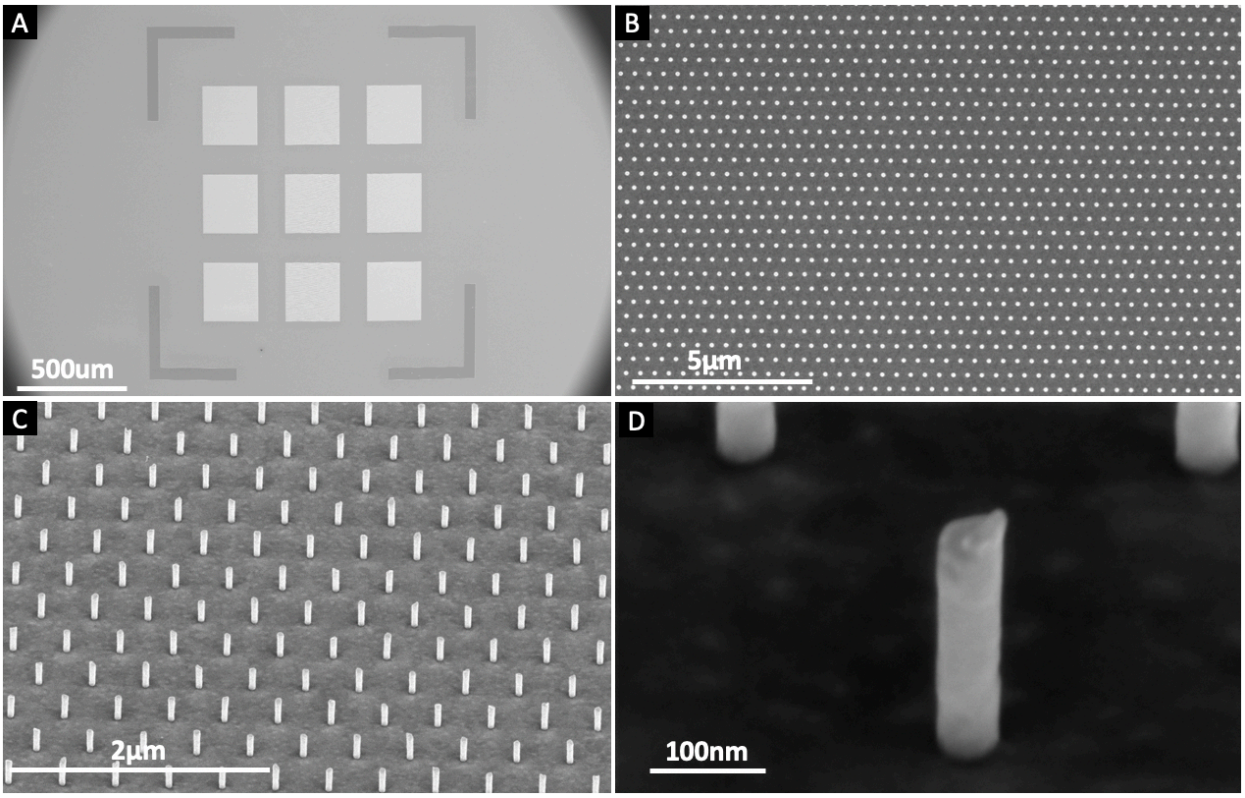

Figure 13. Nanopillar array samples. Each sample contains a 3x3 grid of nanopillar filled pads, each pad 250x250µm and containing nearly 450,000 pillars.

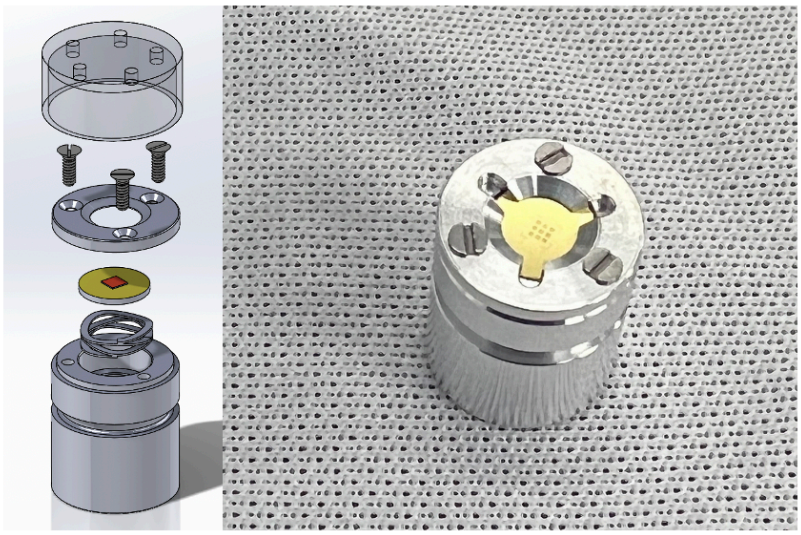

Figure 14. A capsule was developed to hold archaeology type samples for easy handling and installation in ultrapressure vessels with optical access.

Following the palladium electrodeposition on the wafer, a micromachining laser was used to cut out the samples into 5.5mm diameter disks. These disks are then installed in a custom capsule to protect the delicate samples during handling and allow easy installation of the sample into ultrapressure systems (**Fig. 14**). Other than their susceptibility to damage during handling, the nanopillars proved extremely robust during their exposure to 145 ksi gas pressures, and to being loaded and deloaded with protium or deuterium.

These large arrays were never perfect; errors in lithography or electrodeposition would leave occasional gaps in the array. In practice, this was not a serious problem; the errors were rare (typically less than 1 per 1000 pillars). Even more fundamentally, we would record pre-experiment SEM images, allowing us to ignore pre-existing damage when analyzing the experiment. The one form of experimental damage which proved most problematic was due to small debris particles. As a practical matter, most ultrapressure experiments inadvertently included small numbers of "debris" particles (e.g., around a micron in size, and made from silica or hydrocarbons). Gas flow would drive these into the nanopillar arrays; each impact breaking one or more nanopillars. On a global basis, this predation was a small effect, but it was functionally more serious than fabrication errors, because it occurred during the experiment, and could not be discounted by pre-experiment SEM images. A pillar broken or destroyed by an AHE event may be impossible to distinguish from one hurt by a debris particle.

Most of the AHE nanopillar experiments were performed in our Staring apparatus; this is described in detail in the Staring section of the report. To briefly summarize, this apparatus allowed nanopillars to be loaded with either H_2 or D_2 gas at 145 ksi pressures, achieving loadings of 95% or above. The pillars were organized into a grid (usually 3x3) of separated pads, each one a 250 μm square, containing about 450,000 nanopillars. A full experiment therefore, would contain over 4,000,000 nanopillars; each of which acting as a single-event LENR detector.

Obviously, it is impractical for experimenters to personally inspect each pillar in an experiment containing 4,000,000 of them. To deal with this, we developed automated image-processing algorithms (discussed further in the Staring section) to inspect SEM images (acquired both before and after each experiment) and flag "interesting" features for human attention. Two types of filtering were used, one looking for abnormal features (ones that didn't look like normal pillars) and the other for missing pillars.

Usually, the cause of the flagged features was easy to identify. For instance, most missing pillars were already missing in the SEM pre-images; e.g., were due to fabrication errors. Likewise, many of the abnormal features were clearly (due to their size, shape, or position) debris particles, not damaged pillars. Pillars which were found to be missing or damaged in post-experimental SEMs, but not in the pre-images, were always more interesting. However, the cause of these could almost always be identified by one or more "smoking guns". For instance, since an LENR event should mostly affect its host pillar, groups of damaged or missing pillars were indications of handling errors, debris impacts, or (sometimes) too much stimulation energy. And sometimes, assigning

blame to debris particles was clearcut, e.g., the particle was still adjacent to the damage, or several broken pillars lay along a straight line.

After excluding all of these false-positive features, there were usually only a very small number (1 or 2 per experiment) with no obvious cause. However, the fact that they were so rare, were not systematically reproducible, and did sometimes occur with PdH, made it impossible to prove they were caused by LENR. Some could have been, but in each case, they could have been caused by a debris particle which was later carried away with the gas.

This ambiguity meant that nanopillar archaeology was not a definitive tool for either proving or disproving LENR.

Nanostructure Archaeology : Nanofilm Arrays

While nanopillars were too damage prone to give clearcut evidence for or against LENR, the attraction of being able to detect single LENR events remained compelling. So, rather than abandoning archaeology, we simply found a more suitable nanostructure, nanofilms.

These are basically just thin films of Pd, deposited on the surface of an inert substrate. The film is made thin enough (20 – 30 nm) so that energy from an LENR event will blow a hole through the film, down to the substrate; the contrast between the exposed substrate within the hole and the Pd film surrounding it, makes such holes stand out in broad-area SEM imagery.

For convenience in image analysis, we subdivided the Pd film into an array of separate regions, 10 μm squares called nanofilms, with bare substrate in between. Not only did the discrete nature of nanofilms make cataloging locations much simpler and unambiguous, the contrast between the Pd nanofilms and the substrate between them, made it possible to maintain a tight and consistent SEM focus throughout each image sequence.

Nanofilms offer two major advantages over nanopillars; robustness and ease of fabrication.

Thin films are much less vulnerable to damage from handling or debris impacts than are nanopillars. And, when damage does occur, gouging a hole down to the substrate, the shape of the hole hints at its cause, i.e., irregular for debris, smooth and circular for LENR. This, of course, is far different than simply being faced with a missing nanopillar. These facts, that nanofilms experience less damage, and that damage which does occur is informative, mean that nanofilms are a much less ambiguous diagnostic than were nanopillars.

Nanofilms are also much easier to make and can be formed from virtually any metal. Deposition of thin metal films is a very standard and repeatable fabrication process. And, since the individual nanofilms were 10 μm in lateral size, not nanometric, the arrays could be patterned with simple photolithography, not requiring the e-beam lithography used for making nanopillars. Because thin film deposition is a pretty straightforward process, we were able to extend our nanofilm fabrication from Pd films to a wide range of other metals, including many Pd alloys, Ni, and even several rare-earths. In principle, this would have been possible for the electroplating used to make nanopillars,

but in practice, each different composition would have required its own development effort. With nanofilms, switching materials turned out to be quick and straightforward.

In fabrication, a substrate is coated with 1μm thick SPR3612 photoresist over a 200 nm thick liftoff layer. The virtual mask is exposed, and the pattern is developed. Five nm of titanium adhesion layer followed by 25 nm of the desired test material is deposited by e-beam induced evaporation, followed by liftoff of the excess metal. In one case, the nanofilm capacitors used for electrical stimulation in the Chips campaign, we did not use any adhesion layer, since the intent was to apply electric field directly to the palladium surface.

Various substrates were used with these devices depending on the application. In some experimental setups, sapphire wafer substrates were needed due to frequent fracturing of silicon based devices. Sapphire based samples could also employ a 5 nm thick gold layer over the substrate prior to photolithography to aid in charge dissipation during SEM analysis. Thermally oxidized silicon could be used to increase the thermal isolation of the micro pads, but made high resolution SEM imaging challenging and was deemed unnecessary.

For use in LENR experiments, we usually fielded nanofilms in 8x8 arrays; each array forming a separate pad, spaced apart from neighboring pads (**Fig. 15**). Each pad had 64 individual nanofilms, and occupied a 150 μm by 150 μm square. The number of pads, and the separation between them varied depending on the experiment in which they were used. In some cases, e.g., in the Staring campaign, we could tailor our laser beam to match the size of a pad; hence by spacing pads far enough apart, each one could be irradiated with different stimulation conditions. In other experiments, the entire target area received the same stimulation, and so there was no drive to increase pad-to-pad separation.

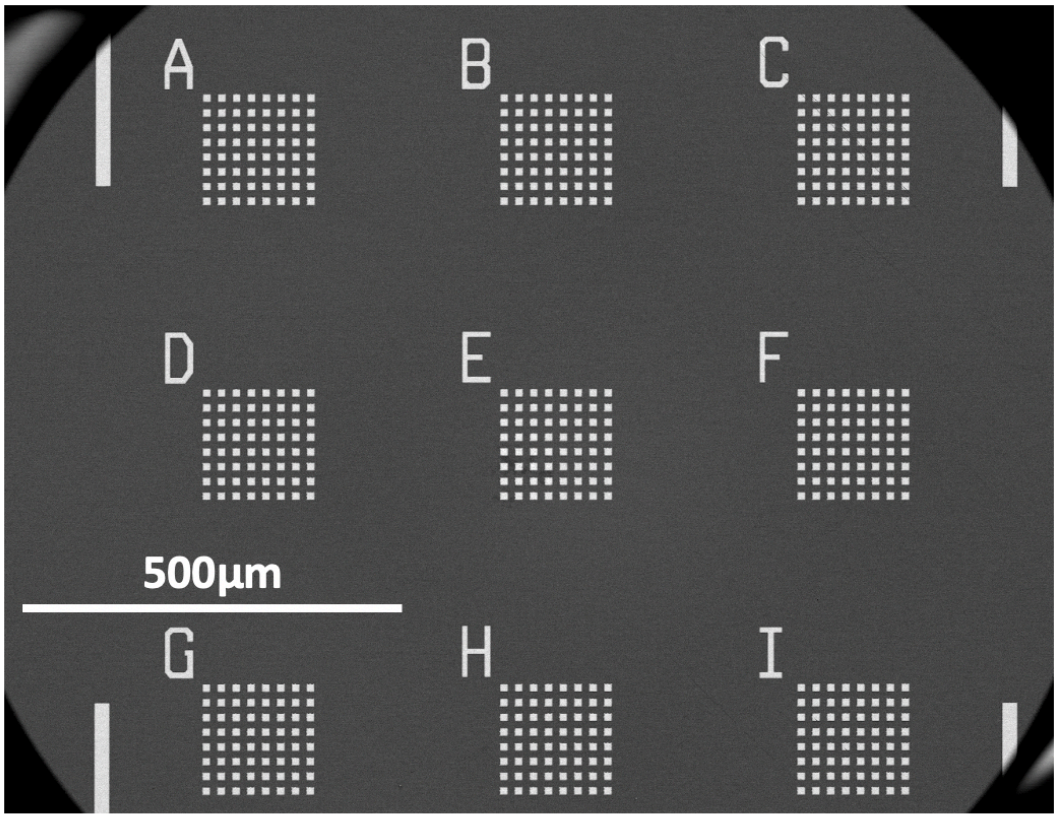

Figure 15. SEM of micro pad array sample.

As mentioned above, a prime reason for splitting large Pd films into arrays of smaller nanofilms, was the ability to identify the locations of interesting features; i.e., in being in a particular nanofilm. The 8x8 array format was chosen to allow us to lithographically mark each individual nanofilm with binary row-column marks, uniquely identifying its location within the array (**Fig. 16**).

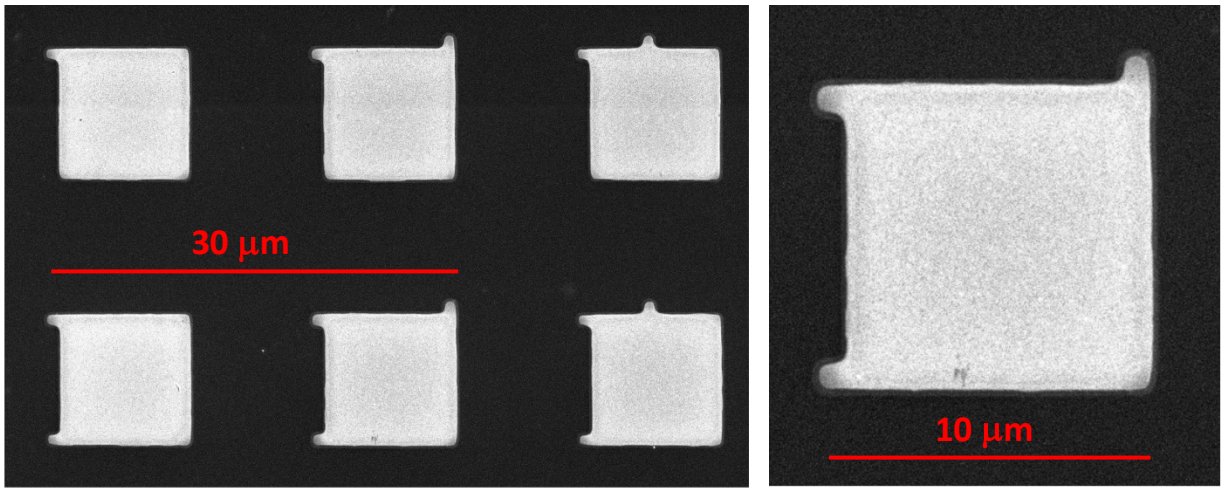

Figure 16. Left: Six nanofilms from rows 4-5 and columns 0-2 of array. Right: Nanofilm (5,1) at row 5, column 1 site of array.

A typical nanofilm experiment involved 576 nanofilms, each 10μm x 10μm in size. We anticipated that LENR events, if present, would be manifested as holes of roughly 0.1 μm in size. These would show up in SEM images of the nanofilm as dark spots against the lighter background of the Pd surface. While we did begin development of a machine-based image analysis tool to search for such holes, in practice it was not essential; human inspection proved effective enough.

The first inspection stage was to simply look at the post-experiment SEM image of each nanofilm, noting the presence of any dark spots. There were typically two causes for these; surface features (debris or contamination), and holes down to the substrate. We used contrast to help distinguish these; holes were black, while surface features were usually not (ranging from white to dark grey). In some cases, black features were clearly irrelevant (e.g., due to scratches or gouges). But, when such causes were not certain, we would refer back to the pre-experiment SEM image of the same nanofilm. Features which were already present before the experiment (**Fig. 17**) were obviously not caused by LENR, while those that only appeared in the post-experimental images potentially were.

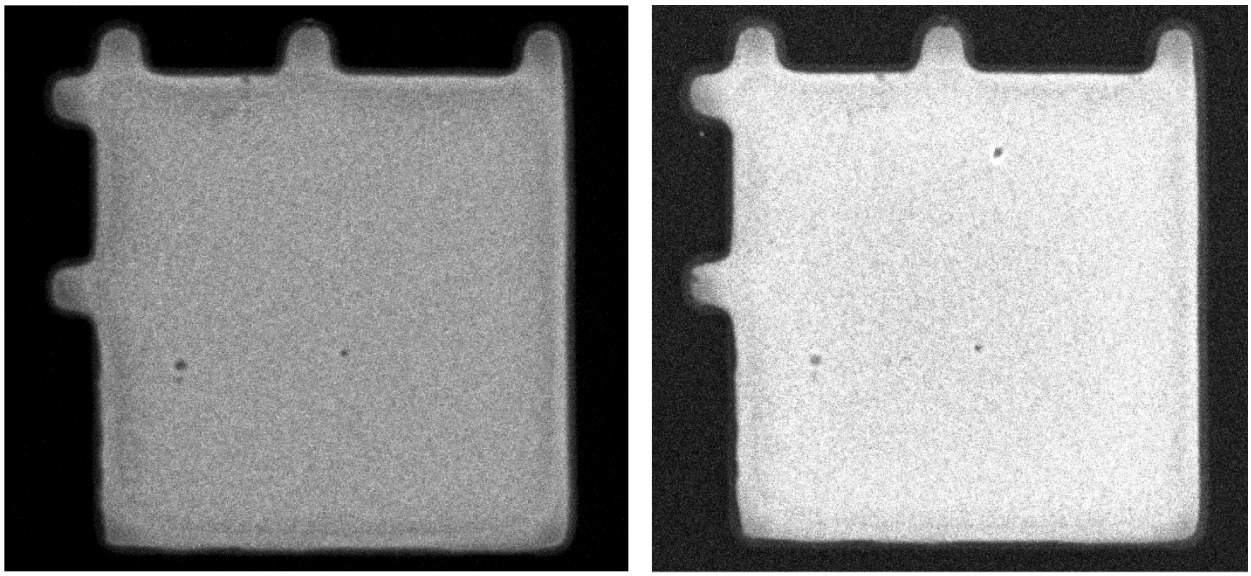

Figure 17. Two SEM images of nanofilm A67 from target BD8508 used in experiment BE4178. On the left is the pre-experimental image, and on the right is the post-experimental one. The lower two spots are present in both images, so are irrelevant to LENR. While the top spot in the post-SEM image is potentially interesting, the white halo around it indicates a debris origin.

After each experiment, there were often image features which could not be explained just from the first-stage inspection. These were black objects (high-contrast compared to the metal film) and only present in the post-experimental SEM view, not the pre-experimental images. We subjected such objects to a second-stage inspection, using spot images with higher magnification and a pair of different SEM detectors (**Fig. 18**), one based upon secondary electron emission, and the other upon electron backscatter. Such images not only addressed the specific features being re-imaged, but also helped us to interpret types of features which could be characterized in the first-stage inspection without needing re-imaging.

Figure 18. Example of second-stage image analysis from BD8508. Top-right: The original post-experimental SEM image of nanofilm A03, with unexplained black spot. Bottom-left: Higher magnification SEM image using backscatter detector. Bottom-right: Higher magnification SEM image using secondary-electron detector. These spot images show that this feature (and similar white-bordered ones) are impact features, not LENR holes.

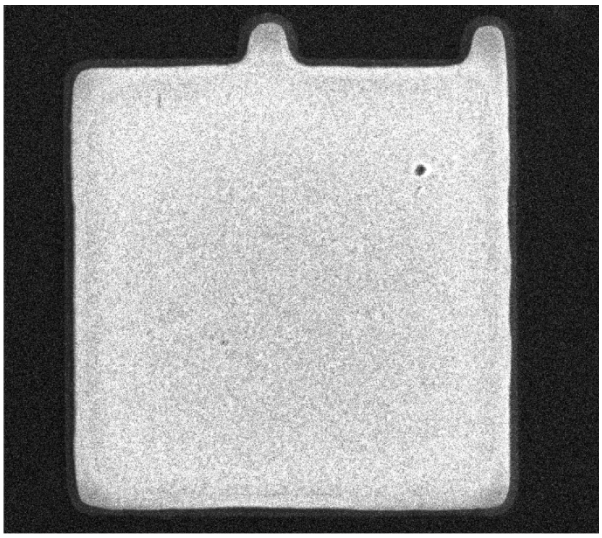

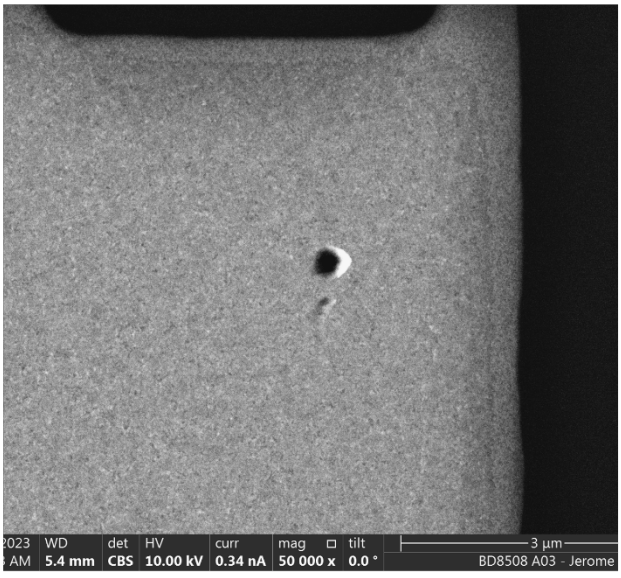

In practice, the time needed to perform nanofilm experiments was dominated not by the actual operational time, but rather by the time required for SEM imaging. Producing a suite of high-resolution SEM images for 9 pads of 8x8 nanofilm arrays (i.e., 576 individual nanofilms) would typically require a full day of SEM time; and, of course, mean forgoing other usage for that period. Performing a fully documented and controlled experiment required 4 such imaging periods; having each PdD experiment matched with a corresponding PdH one, and with all nanofilms SEM-imaged both before and after the experiment. Because of this large resource commitment, we sometimes used a shortcut procedure to increase throughput four-fold, in which only post-imaged PdD versions were performed. The rationale in these cases, was that in the event that PdD nanofilms were not showing interesting results in post-experiment SEM images, there was little need to expend time on taking pre-experimental images, or to running PdH control versions.

Nanostructure Archaeology : Nanofilm Experiments

We used nanofilm arrays as single-event detectors in a wide range of different LENR experiments.

The first three cases, listed below, were our most extensive applications of nanofilm archaeology. All of them tested not just pure Pd, but also five different Pd alloys (Pd with B, Ni, Ag, Rh, Pt).

Staring: In this case, the Staring laser was used as a stimulation source, providing thermal stimulation at 145 ksi with two different laser wavelengths, and a variety of intensities and durations. The results, and usage of nanofilms, are described in much further detail in the Staring section of this report.

Ultra-Short-Pulse: We used nanofilm arrays to test for LENR in the extreme environment of both ultra-high pressure and non-thermal stimulation (using the Ekspla femtosecond laser). A tabulation of these experiments is given in Table 1 of the Ultra-Short-Pulse section of the report.

High Temperature Equilibrium: We used nanofilm arrays to test for LENR in an extreme form of pressure-temperature equilibrium; ultra-high pressure and near-melting temperature. A tabulation of these experiments is (as above) given in Table 1 of the Ultra-Short-Pulse section of the report.

The three cases above involved many experiments, each containing 576 nanofilms. Most of the nanofilms showed no hole-like features. When features were observed, they were individually inspected and categorized, as described earlier. Most of the pure Pd targets were pre-imaged, so many "suspicious" features in post-images could definitively explained. Many of the alloy experiments were not pre-imaged, which meant that this sieve method was not available for some of the observed features. However, in the course of our image analysis, we learned a lot about the appearance of surface debris and impact damage, and how to use image shape and contrast to distinguish them from AHE-type holes. In the course of these three types of experiments we saw no features which appeared to be caused by LENR events.

The following four cases were less extensively pursued, and used only pure Pd targets, not any of its alloys.

Heater Pad Stimulation: This set of experiments placed arrays of nanofilms onto resistively heated pads in a chip format. Functionally, this is similar to the Staring experiments discussed above; still thermal stimulation, but applied resistively rather than by a laser. These tests were discussed in the Chip section of this report.

Cryogenic: In this experiment (BE4131) we used no explicit stimulation; the goal was to look for LENR in a cryogenic situation. The sample was loaded in 145 ksi D_2 and held at -160ºC for 12 hours, so it formed stoichiometric PdD, having very little thermal stimulation, but a greater chance of Bose-Einstein effects than in other cases.

Electric Field Stimulation: In some experiments, we used the electrical capacitor arrays, described in the Chips section of this report, for nanofilm archaeology. These looked for single

LENR events caused by intense electric fields (both static and oscillatory). Operationally, these archaeological tests were similar to our normal capacitive ones, the only difference being the introduction of high resolution SEM imaging.

High Pressure Electrochemistry: After developing nanofilm archaeology, we naturally wanted to use it to look, with single-event sensitivity, for LENR caused by electrolytic loading, not just the gas-loading that all our other nanofilm experiments used. We employed the same type of linked-together Pd nanofilm arrays developed for the Chip capacitor tests as the cathodes for high-pressure D_2O-based electrochemistry.

As these arrays are different from those used for gas-loaded experiments, they're shown below (**Fig. 19**), along with one of the nanofilms as it appeared after the experiment.

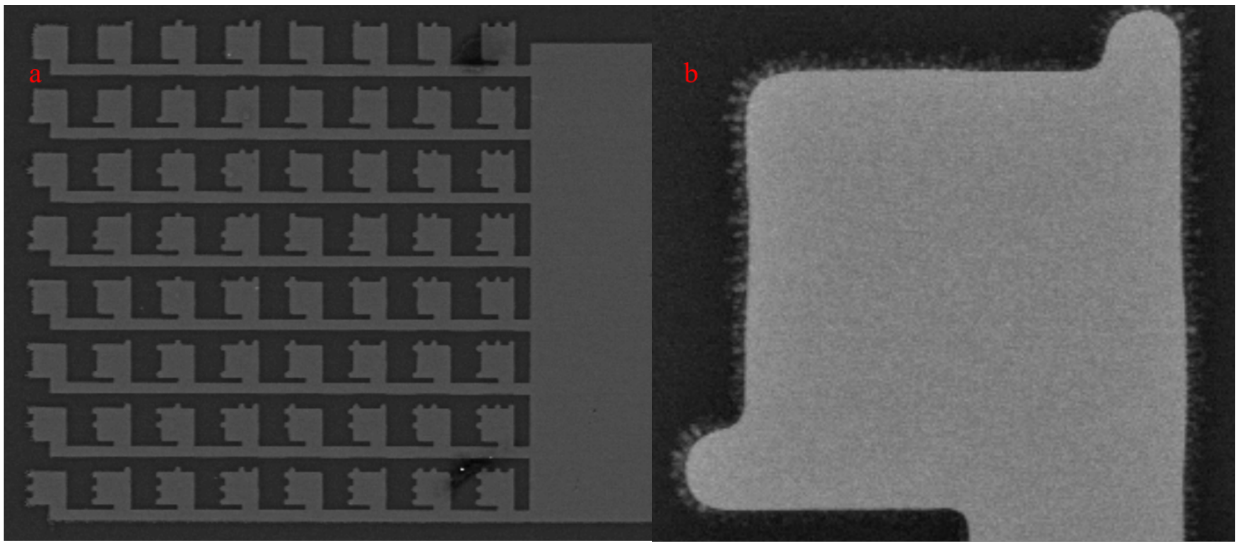

Figure 19. Post-experimental SEMs for BE4199. (a) The 64 linked-together nanofilms of pad C. (b) Nanofilm C11. Note the filamentary features extending from the edges of the nanofilm.

While not as extensive as the three upper cases of nanofilm archaeology experiments, none of these four types of experiments detected any signs of LENR events.